Journal of Applied Physics

Transducerless time domain reflectance measurement of semiconductor thermal properties

Cite as: J. Appl. Phys. **131**, 025101 (2022); https://doi.org/10.1063/5.0069360
Submitted: 30 August 2021 • Accepted: 14 December 2021 • Published Online: 10 January 2022

Sarah Warkander and Junqiao Wu

COLLECTIONS

Note: This paper is part of the Special Topic on Engineering and Understanding of Thermal Conduction in Materials.

EP This paper was selected as an Editor's Pick

Journal of Applied Physics
SPECIAL TOPIC:
Shock Behavior of Materials
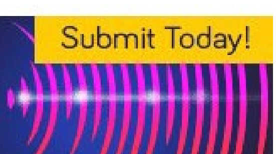

© 2022 Author(s).

Journal of Applied Physics ARTICLE scitation.org/journal/jap

Transducerless time domain reflectance measurement of semiconductor thermal properties

Cite as: J. Appl. Phys. **131**, 025101 (2022); doi: 10.1063/5.0069360
Submitted: 30 August 2021 · Accepted: 14 December 2021 ·
Published Online: 10 January 2022

Sarah Warkander[1] and Junqiao Wu[1,2,a)]

AFFILIATIONS

[1]Department of Materials Science and Engineering, University of California, Berkeley, California 94720, USA
[2]Materials Sciences Division, Lawrence Berkeley National Laboratory, Berkeley, California 94720, USA

Note: This paper is part of the Special Topic on Engineering and Understanding of Thermal Conduction in Materials.
[a)]**Author to whom correspondence should be addressed:** wuj@berkeley.edu

ABSTRACT

The dominant techniques for laser-based thermal measurement, time-domain thermoreflectance (TDTR) and frequency-domain thermoreflectance, generally require that samples be coated with a metal transducer layer. The properties of the transducer and its interface to the sample are then important to the interpretation of results, and heat conduction in the transducer layer can limit measurements of ultra-thin samples or in-plane conductivity. We demonstrate the feasibility of measuring semiconductor samples using standard TDTR instrumentation, without the use of a metal transducer. A mathematical model accounting for non-zero laser penetration depth as well as both thermal and charge carrier effects is presented, and the ability of the model to describe and fit to experimental data for silicon and germanium samples is demonstrated. Though at this stage measurement uncertainties are larger than for traditional TDTR, we anticipate that the use of this technique will expand the range of samples that can be measured with existing TDTR setups.

Published under an exclusive license by AIP Publishing. https://doi.org/10.1063/5.0069360

INTRODUCTION

The question of how to effectively and accurately measure the thermal properties of materials is a long-standing one. Standard approaches are based on applying heat and monitoring its diffusion and then comparing the measured result to a thermal model.[1] Local measurements require establishing a thermal diffusion length, for example, through the use of a modulated heat source. For decades, techniques based on heating via a modulated laser beam have been used, with the measurement of the sample response via the photoacoustic effect,[2,3] through photothermal deflection,[4,5] with piezoelectric transducers,[6] or based on reflectivity changes.[7–10] In recent years, time- and frequency-domain thermoreflectances (TDTR[11] and FDTR,[12] respectively) have become the dominant approaches. TDTR and FDTR rely on temperature-driven changes in the optical reflectivity of the sample surface,[13] allowing monitoring of temperature changes through the change in reflected intensity of a second laser beam. By detecting the modulation in reflection corresponding to the modulated heating, the thermal response of the sample can be determined.

In their usual applications, both TDTR and FDTR involve the deposition of a thin metal transducer layer on the sample to be measured. This transducer is then the only layer that interacts with either of the incident laser beams, acting as both heater and thermometer for the rest of the sample. The use of a transducer allows the assumption that the change in reflection is directly related to the sample surface temperature as the primary component affecting the reflectivity of metals is the distribution of free electrons, which is temperature dependent.[14] With an appropriate selection of metal and laser wavelength, the coefficient of thermoreflectivity, dR/dT, can be substantially larger than that in an unoptimized system.[15] Additionally, the optical penetration depth of the laser in the metal transducer layer is small, allowing heating to be modeled as occurring at the surface.

However, requiring a metal transducer layer adds complexity and can limit measurement. Deposition of the transducer is a permanent modification of the sample surface, removing the possibility of *in situ* measurements. In interpreting results, additional parameters, such as the thickness and heat capacity of the transducer and the thermal interface conductivity to the sample, become important. The conductivity of the transducer-sample interface must be high enough compared to the conductivity of the sample for the measurement to be sensitive to sample properties. For ultra-thin samples or

Published under an exclusive license by AIP Publishing

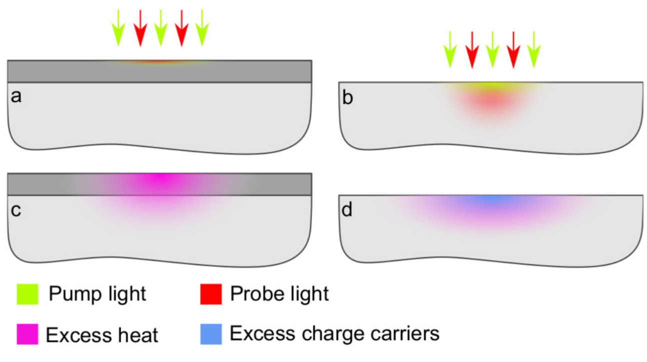

FIG. 1. (a) In a transducer-coated sample, light absorption happens near the surface of the material, whereas in (b) an uncoated semiconductor sample, light penetrates into the material. (c) In a coated sample, heat must diffuse through the transducer to reach the sample, and no charge carriers are generated. (d) In an uncoated sample, heat and charge carriers are both generated and diffuse directly in the sample.

measurements of in-plane conductivities, the transducer acts as a thermal short and suppresses the sensitivity of the measurement to the properties of interest, especially for samples with relatively low thermal conductivities.[16] Thus, a technique that does not require a transducer layer is desirable. Key differences between measurements with and without a transducer are highlighted in Fig. 1.

Others have pursued the goal of transducerless thermoreflectivity measurements. Wang *et al.*[14] and Qian *et al.*[16] demonstrated the feasibility of FDTR measurements on uncoated samples; however, their thermal model breaks down at short delay times and in materials with long carrier diffusion lengths. Tanaka *et al.*[17] use a TDTR-like setup but use a thermal model that is only valid for time scales shorter than those used in many TDTR measurements. By using overlapped pump and probe beams, we avoid the complex optical systems required for the beam-offset techniques of Fournier *et al.*[1] and Hurley *et al.*[8] In this paper, we demonstrate the usage of standard TDTR instrumentation and measurement technique to determine thermal conductivities of semiconductors without the use of a transducer layer. We anticipate that such a technique can extend the range of samples, which can practically be measured using existing TDTR equipment.

TRANSDUCERLESS MEASUREMENTS

The mechanism of TDTR measurements is described in detail elsewhere.[11] TDTR is a pump–probe method in which an ultrafast pulsed laser is divided into two beams, both of which are directed to a sample. Our TDTR setup uses a 565 nm pump beam and an 800 nm probe beam. The pump beam is modulated, typically at a frequency of 0.1–10 MHz, and the probe beam is passed through a mechanical delay stage, temporally separating the incidences of the pump and probe beams by some delay time—in our setup, up to 3 ns. This allows measurement both over the fast (picosecond to nanosecond) timescale of the delay stage and over the slow (microsecond) timescale of the pump modulation.

In transducerless time-domain reflectivity measurements, both pump and probe beams are incident directly on the semiconductor sample. We highlight the key processes that occur when a pump pulse strikes our samples in Fig. 2. In our experiments, the pump beam photon energy, $h\nu$, is greater than the bandgap of our samples, E_g, and the pump has a non-zero penetration depth. When a pump pulse is absorbed, electron–hole pairs with energy $h\nu$ are generated throughout a volume of the sample corresponding to the region of absorption. Within a few picoseconds, excited carriers thermalize to the lattice temperature and relax to the band edge,[18,19] releasing thermal energy ($h\nu - E_g$). Over the next tens of picoseconds to hundreds of nanoseconds, the photogenerated carriers and the generated heat diffuse into the sample, and the carriers recombine. Assuming primarily non-radiative recombination, this leads to an additional source of thermal energy E_g for each recombination event, serving as an additional distributed heat source. Beyond the photocarrier lifetime, the population of carriers returns to its background level, leaving only the thermal energy which continues to diffuse. At long enough timescales, sufficient spreading of the thermal pulse has occurred that the sample can be treated as having returned to equilibrium. Crucially, for intermediate time scales (nanosecond to microsecond, depending on carrier recombination time), continued heating arising from carrier recombination means that proper treatment of the sample temperature requires consideration of both generation and diffusion of heat and the behavior of the photoexcited charge carrier population. Accordingly, we coin the term transducerless time-domain reflectance (tTDR), highlighting that changes in optical reflectance are modulated both thermally and electronically, as opposed to only thermally as in TDTR. As with traditional TDTR, the sensitivity of the measurement to sample

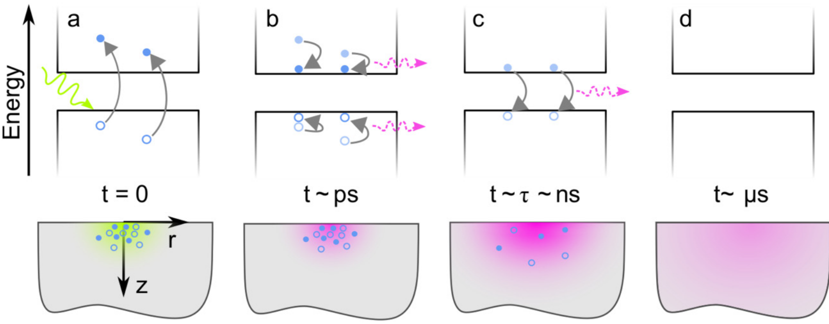

FIG. 2. Schematic of the processes occurring after a pump pulse strikes a semiconductor sample. (a) Electron–hole pairs are generated near-immediately; (b) carriers thermalize rapidly, generating heat; (c) heat diffuses and carriers diffuse and recombine, generating more heat; (d) heat continues to diffuse after carriers have fully recombined.

Published under an exclusive license by AIP Publishing

responses across multiple timescales is beneficial—we are able to measure thermal effects both at short delay times, where the sample response is strongest, and at long times when electronic effects are diminished. Additionally, though we do not explore it in this work, we anticipate that the sensitivity of tTDR to both thermal and electronic effects could be used to probe links between variations in thermal and electronic properties of materials.

Various authors have approached the problem of describing coupled thermal and carrier behavior following laser incidence. Stearns and Kino[6] and Fournier *et al.*[4] solve for the special case with near-surface carrier generation. Sablikov and Sandomirskii[3] solve for the carrier concentration in the sample and the surface temperature caused by a non-zero pump penetration, but do not give an expression for temperature below the surface. Tanaka *et al.*[17] extend the model of Sablikov and Sanomirskii to temperature as a function of depth but do not consider heat generation from carrier recombination. All these authors assume that the laser spot is large enough to treat its lateral dimensions as infinite, which eliminates the possibility of measuring sample anisotropy. Yang *et al.*[20] and Qian *et al.*[16] consider spots with finite lateral dimensions and non-zero pump penetration but model only the thermal diffusion from the initial laser incidence, neglecting carrier effects. Here, we consider the full case where the pump laser has a finite size, penetrates into the sample, and generates free charge carriers that recombine as a further heat source.

Carrier and temperature behavior

The behaviors of both the excited carriers and the temperature field are governed by diffusion equations. As discussed above, the temperature field depends on the carrier concentration; in principle, the carrier population is also a function of temperature. However, we assume that the temperature excursions of our samples are small enough that the population of carriers generated due to increased temperature is small compared to the photoexcited population, making this effect negligible and allowing the carrier equation to be solved separately from the temperature equation. To validate this assumption, we find an upper bound on the per-pulse heating by assuming the full energy of the pump beam is converted to heat in the volume in which it is absorbed. For the experimental parameters used in this work, we expect approximately 2 K of temperature rise for germanium and 0.2 K for silicon, corresponding to an increase in intrinsic carrier concentration of 2×10^{12} and $1 \times 10^{8}\,\mathrm{cm^{-3}}$, respectively.[21,22] Additionally, we assume that the photocarrier population is large enough to dominate over the background doping so that the total electron and hole populations are similar, that is, $N \approx P$. For our measurements, the pump energy per pulse was approximately 10^{-10} J, corresponding to an initial photoexcited carrier concentration of approximately $1.0 \times 10^{19}\,\mathrm{cm^{-3}}$ in germanium and $1.4 \times 10^{19}\,\mathrm{cm^{-3}}$ in silicon. Figure 3 highlights the degree to which the photoexcited concentration outweighs carrier concentrations due to both temperature changes and the light doping of the samples measured.

A full treatment of the recombination of excited carriers would require consideration of one, two, and three phonon

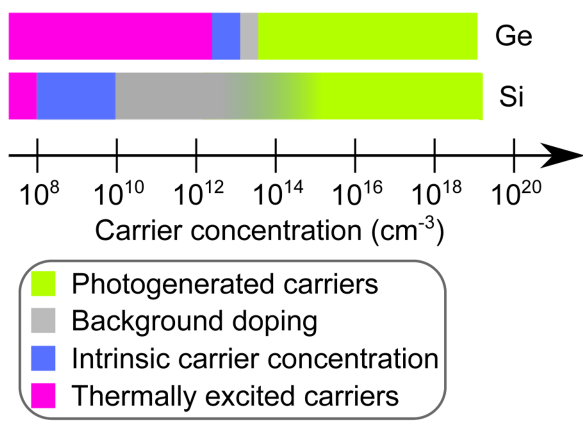

FIG. 3. Carrier concentrations in germanium and silicon samples. With the experimental parameters used in this study, the density of photoexcited carriers far exceeds the intrinsic carrier concentration, the background doping of the sample, and the population of carriers generated due to the increase in sample temperature, validating the assumptions of our model. The background doping for the silicon sample is shown as a range because the sample was too resistive to directly measure the doping level.

processes, yielding

$$\frac{\partial N_{\mathrm{recomb}}}{\partial t} = -\gamma_1 N - \gamma_2 N^2 - \gamma_3 N^3, \tag{1}$$

where γ_1, γ_2, and γ_3 are the carrier recombination rates for linear, two-body, and Auger processes, respectively.[17] Considering the full form of this equation is not mathematically feasible, but given the relatively high photoexcited carrier concentrations of our measurements, we expect Auger recombination to dominate at small delay times. Following the approach of Tanaka *et al.*,[17] we approximate

$$\frac{\partial N_{\mathrm{recomb}}}{\partial t} = -\frac{N}{\tau}, \tag{2}$$

where

$$\tau = 1/\gamma_3 N_0^2, \tag{3}$$

with N_0 being the initial carrier concentration.

We begin by considering the impulse response of the sample. Each laser pulse is short enough to be modeled as a delta function in the time domain, so, considering a Gaussian pump laser spot with penetration depth $1/\alpha$ and radius w_0, we write the intensity in the sample as

$$A_{\mathrm{pump}} = A_0 \mathrm{e}^{(-2r^2/w_0^2)} \mathrm{e}^{-\alpha z} \delta(t), \tag{4}$$

where A_0 is a constant coefficient representing the incident intensity of the pump laser.

The excess carrier concentration caused by the laser, N, is described by a diffusion equation with generation due to the laser

Published under an exclusive license by AIP Publishing

spot and loss due to recombination. Carrier motion caused by driving forces other than diffusion is assumed to be negligible. To confirm this, we estimate the current density caused by thermoelectric effects as

$$J_S = S\sigma\alpha\Delta T, \tag{5}$$

with S being the Seebeck coefficient, σ being the electrical conductivity of the sample, α being the absorption rate of the pump laser, and ΔT being the temperature deviation caused by the laser incidence. The diffusion current density is estimated from the electrical diffusivity, D; the absorption rate of the pump laser, α; and the concentration of photoexcited carriers, ΔN, as

$$J_D = eD\alpha\Delta N, \tag{6}$$

with e being electron charge. For our germanium and silicon samples, we expect J_S to be 2×10^5 and 1×10^3 A/m^2,[23,24] whereas J_D will be 4×10^8 and 1×10^9 A/m^2, showing that diffusion dominates the carrier motion.

For modeling carrier diffusion, we assume in-plane diffusivity, D_r, to be independent of the direction but allow it to be different from the out-of-plane diffusivity, D_z, yielding

$$-D_z\frac{\partial^2 N}{\partial z^2} - D_r\frac{1}{r}\frac{\partial}{\partial r}\left(r\frac{\partial N}{\partial r}\right) + \frac{\partial N}{\partial t} = \frac{-N}{\tau} + \frac{A_0}{\pi w_0^2}\delta(t)e^{-2r^2/w_0^2}\mathrm{e}^{-\alpha z}, \tag{7}$$

where τ is the time constant of carrier recombination.

Assuming a semi-infinite material with surface recombination velocity s at its free surface, we find boundary conditions

$$\lim_{z\to\infty} N = 0, \tag{8}$$

$$D_z\frac{\partial N}{\partial z}\bigg|_{z=0} = sN|_{z=0}. \tag{9}$$

We convert the partial differential equation to an ordinary differential equation in z by taking the Hankel transform (in r) and Fourier transform (in t), eliminating the derivatives in r and t, respectively, and replacing $\delta(t)$ with

$$-D_z\frac{d^2N}{dz^2} + D_r k^2 N + \mathrm{i}\omega N = \frac{-N}{\tau} + \frac{A_0}{4\pi}\mathrm{e}^{-k^2w_0^2/8}\mathrm{e}^{-\alpha z}. \tag{10}$$

This is solved by

$$N(z,\omega,\ k) = \frac{A_0}{4\pi D_z}\mathrm{e}^{-k^2w_0^2/8}\frac{1}{q^2-\alpha^2}\left(\mathrm{e}^{-\alpha z} - \frac{s+D_z\alpha}{s+D_z q}\mathrm{e}^{-qz}\right), \tag{11}$$

with

$$q^2 = (D_r k^2 + \mathrm{i}\omega + 1/\tau)/D_z. \tag{12}$$

Equations (11) and (12) represent the frequency response of the excess carrier concentration, in the Hankel transform domain.

The excess temperature, T, is described by a diffusion equation with generation due to both the laser spot and carrier recombination. We treat the thermal conductivity as constant with time, neglecting variation caused by the pump incidence. For the germanium and silicon samples studied here, the increase in thermal conductivity due to increased carrier concentration was estimated from the Wiedemann–Franz Law to be less than 0.5%.

As we did for the electrical diffusivity, we assume that in-plane thermal conductivity Λ_r is independent of the direction but not necessarily identical to out-of-plane conductivity Λ_z and write

$$-\Lambda_z\frac{\partial^2 T}{\partial z^2} - \Lambda_r\frac{1}{r}\frac{\partial}{\partial r}\left(r\frac{\partial T}{\partial r}\right) + c_p\frac{\partial T}{\partial t} = \frac{E_g}{\tau}N + \frac{A_0}{\pi\omega_0^2}(h\nu - E_g)\delta(t)\mathrm{e}^{-2r^2/w_0^2}\mathrm{e}^{-\alpha z}, \tag{13}$$

where c_p is the heat capacity of the sample, E_g is the bandgap, and $h\nu$ is the energy of a pump photon.

With the same assumptions as above, the boundary conditions are

$$\lim_{z\to\infty} T = 0, \tag{14}$$

$$-\Lambda_z\frac{\partial T}{\partial z}\bigg|_{z=0} = E_g sN|_{z=0} \tag{15}$$

and following the same approach of taking Hankel and Fourier transforms and then solving the ODE, find

$$T(z,\omega,\ k) = \frac{A_0}{4\pi\Lambda_z}\mathrm{e}^{-k^2w_0^2/8}(\mathrm{e}^{-z\alpha}C_1 + e^{-qz}C_2 + \mathrm{e}^{-q_{th}z}C_3), \tag{16}$$

where

$$q_{th}^2 = (\Lambda_r k^2 + c_p\mathrm{i}\omega)/\Lambda_z, \tag{17}$$

$$C_1 = \frac{-(E_g - h\nu)}{q_{\mathrm{th}}^2-\alpha^2} + \frac{E_g}{D_z\tau(q_{\mathrm{th}}^2-\alpha^2)(q^2-\alpha^2)}, \tag{18}$$

$$C_2 = \frac{E_g}{D_z\tau(q^2-q_{\mathrm{th}}^2)(q^2-\alpha^2)}\frac{s+D_z\alpha}{s+D_z q}, \tag{19}$$

$$C_3 = \frac{-1}{q_{th}}\left[\frac{-\alpha(E_g-h\nu)}{q_{th}^2-\alpha^2} + \frac{1}{(q^2-\alpha^2)D_z\tau}\left(-E_g s\tau + \frac{s+D_z\alpha}{s+D_z q}\left(E_g s\tau + \frac{E_g q}{q^2-q_{\mathrm{th}}^2}\right) + \frac{E_g\alpha}{q_{\mathrm{th}}^2-\alpha^2}\right)\right]. \tag{20}$$

Published under an exclusive license by AIP Publishing

Equations (16)–(20) give the frequency response of the excess sample temperature, in the Hankel transform domain.

To highlight the types of solutions generated by Eqs. (11) and (16), we calculate the delay time dependencies for the response to a single pump pulse and plot the resulting solutions in Fig. 4.

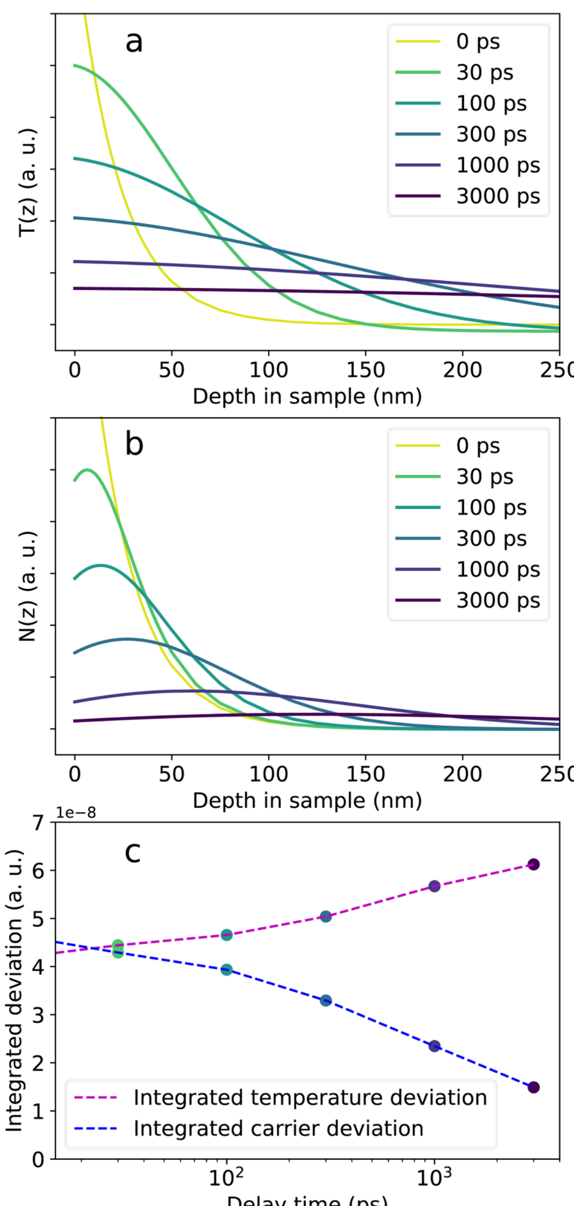

FIG. 4. Plots of the results of (a) Eq. (16) and (b) Eq. (11) for a germanium sample, transformed to the time domain for a single laser pump pulse. At zero delay time, curves match the exponential behavior of the pump distribution but diffuse into the sample as time passes. Additionally, the carrier concentration dies away and more heat is generated by recombination, as shown by (c) the changing area under the curve.

At zero delay time, the depth profiles of both the temperature and the carrier distributions match that of the pump spot, and as time increases carriers and heat diffuse into the sample, but at different rates. Additionally, carrier recombination both in the bulk and at the surface decreases the total carrier concentration and increases the total temperature deviation. At long enough delay times, the carrier concentration will decay to zero and the total temperature deviation will plateau.

Reflectivity

We now consider the effect of the probe beam. We assume it to be Gaussian in the transverse direction with radius w_1 and have penetration depth δ_1 into the sample, allowing its intensity to be described by

$$A_{\text{probe}} = A_1 e^{(-2r^2/w_1^2)} e^{-z/\delta_1}, \tag{21}$$

where A_1 is a constant coefficient representing the incident intensity of the probe laser.

The total reflectivity is a function of the complex refractive index, $\tilde{n} = n + i\kappa$, in the entire volume addressed by the probe. We first consider the z dimension.

To properly address the reflectivity of the sample to the penetrating probe beam, it is necessary to solve Maxwell's equations in the material. We seek to consider the effects of both carrier concentration and temperature, so we begin by assessing the response to an arbitrary parameter affecting $\tilde{n}$, which we denote $\phi(z, \omega)$. For such a parameter, we expect a change in reflection,[25]

$$\Delta R(\omega) = \int_0^\infty f(z)\phi(z, \omega)\mathrm{d}z, \tag{22}$$

where $f(z)$ is a sensitivity function consisting of an exponentially damped oscillation caused by the interference of reflections from the surface and within the sampled depth[25]

$$f(z) = f_0\left(\frac{\partial n}{\partial \phi}\sin\left(\frac{4\pi nz}{\lambda} - \theta\right) + \frac{\partial \kappa}{\partial \phi}\cos\left(\frac{4\pi nz}{\lambda} - \theta\right)\right)e^{-z/\delta_1}, \tag{23}$$

$$f_0 = 8\frac{2\pi\left(n^2(n^2+\kappa^2-1)^2 + \kappa^2(n^2+\kappa^2+1)^2\right)^{1/2}}{\lambda\left((n+1)^2+\kappa^2\right)^2}, \tag{24}$$

$$\tan\,\theta = \frac{\kappa(n^2+\kappa^2+1)}{n(n^2+\kappa^2-1)}, \tag{25}$$

where λ is the probe wavelength and $\theta \in \left[0, \frac{\pi}{2}\right]$. For the semiconductors under study here, $\frac{\partial \kappa}{\partial \phi} \ll \frac{\partial n}{\partial \phi}$, so, to a good approximation

$$f(z) = f_0\left(\frac{\partial n}{\partial \phi}\sin\left(\frac{4\pi nz}{\lambda} - \theta\right)\right)e^{-z/\delta_1}, \tag{26}$$

which is plotted in Fig. 5.

Published under an exclusive license by AIP Publishing

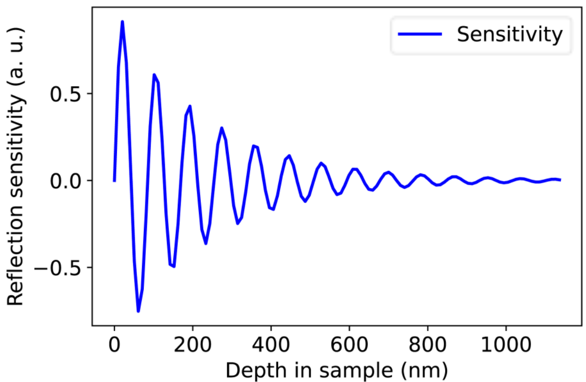

FIG. 5. The result of Eq. (26), the sensitivity of the reflectivity of the sample to deviations in carrier concentration and temperature, as a function of depth. θ is taken to be zero, corresponding to the case of negligible κ and $\frac{\partial \kappa}{\partial \phi}$, and all other parameters are those of germanium probed at 800 nm.

We now consider how to define $\phi(z, \omega)$. In semiconductors, the refractive index is affected by both the carrier and thermal distributions,[17]

$$\Delta n = \frac{\partial n}{\partial T}\Delta T + \frac{\partial n}{\partial N}\Delta N, \tag{27}$$

so instead of the single parameter ϕ, we must consider both N and T, yielding

$$\Delta R(\omega, k) = \int_0^\infty f_0 \sin\left(\frac{4\pi n z}{\lambda} - \theta\right) \times \left(\frac{\partial n}{\partial N}\Delta N(\omega, z, k) + \frac{\partial n}{\partial T}\Delta T(\omega, z, k)\right) e^{-z/\delta_1} dz. \tag{28}$$

This adds two additional unknown parameters to the system, $\frac{\partial n}{\partial N}$ and $\frac{\partial n}{\partial T}$. The first, $\frac{\partial n}{\partial N}$, can be estimated from the semiconductor Drude equation[26]

$$\frac{dn}{dN} = \frac{-\lambda^2 e^2}{2\pi n m^* c^2}, \tag{29}$$

where λ is the probe wavelength, e is the charge of an electron, m^* is the ambipolar effective mass of the charge carriers, and c is the speed of light.

The second term, $\frac{\partial n}{\partial T}$, is a result of several effects, including Fermi smearing, electron–phonon collisions, and bandgap shift, and is best estimated from empirical data.[17] However, due to the number of difficult-to-estimate initial coefficients of our equation, we fit a normalized version of the signal such that only the ratio $\frac{\partial n}{\partial N}/\frac{\partial n}{\partial T}$ is relevant to the final result and can be determined in the data fitting process. In most semiconductors, $\frac{\partial n}{\partial T}$ is positive, unlike $\frac{\partial n}{\partial N}$, so $\frac{\partial n}{\partial N}/\frac{\partial n}{\partial T}$ is expected to be negative.[17]

We now consider the lateral extent of the probe. The probe measures a weighted average of the area it strikes.[11] Taking the Hankel transform of Eq. (21) and combining with the Hankel domain solution $\Delta R(\omega, k)$, we find

$$\Delta R_{\text{probe}}(\omega) = \int_0^\infty \Delta R(\omega, k) e^{-k^2 w_1^2/8} k \, dk. \tag{30}$$

Combined with Eqs. (11), (12), (16)–(20) and (28), (30) gives an expression for the frequency dependence of the measured reflectivity.

Voltage signal

As described above, the measured tTDR signal is given by the reflection of a modulated pulsed laser. The reflection is directed to a photodetector, which provides a voltage signal which is sent to a lock-in amplifier set to the modulation frequency, f. This means that the signal samples the frequency response of the sample at $\pm f$ as well as at frequencies shifted by multiples of the frequency of the laser repetition rate, $1/\tau_{rep}$,[11]

$$\Delta V(t_{\text{delay}}) = \frac{dV}{dR} \sum_{m=-\infty}^{\infty} \left(\Delta R\left(\frac{m}{\tau_{rep}} + f\right) + \Delta R\left(\frac{m}{\tau_{rep}} - f\right)\right) \times \exp(2\pi i m t_{\text{delay}}/\tau_{rep}), \tag{31}$$

where ΔV is the measured voltage signal and $\frac{dV}{dR}$ is the responsivity of the photodetector-amplifier system. By combining Eqs. (30) and (31), we find the predicted tTDR signal. An example of the depth profiles of T and N and their combination into the final signal is shown in Fig. 6.

RESULTS

We validate our time-domain approach to tTDR measurements by confirming our ability to measure known samples. Here, we focus on germanium and silicon, both indirect-bandgap semiconductors with bandgaps below the energy of our 565 nm pump and 800 nm probe beams. We assume that carrier recombination happens primarily through non-radiative mechanisms, validating our assumption that each recombination event releases thermal energy E_g. We measure [100] wafers of both materials.

As is typical for TDTR, we perform measurements at a range of modulation frequencies and fit our results for each frequency independently (Table I). Optical penetration depths and refractive indexes were determined by ellipsometry, and comparison to literature values shows good agreement. Electronic diffusivity was determined through Hall effect measurements for germanium and as a fitting parameter for silicon. In both cases, diffusivities were found to be lower in our samples than in the literature, more notably for germanium, which we attribute to lower purity of our samples than those studied elsewhere. The range of diffusivity considered for germanium spans the standard deviation of the values found through repeated Hall measurement, and for silicon, the range covers the values found from fitting at different modulation frequencies. Data fitting for silicon are described in more detail

Published under an exclusive license by AIP Publishing

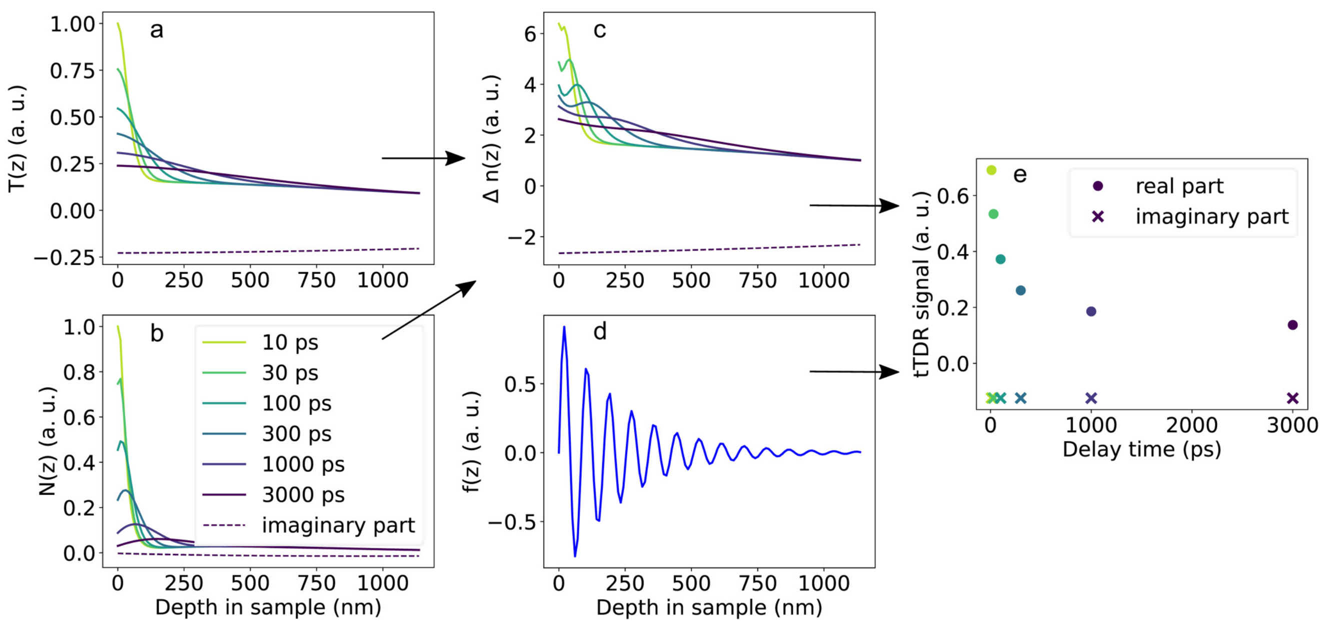

FIG. 6. Schematic of temperature profile and carrier concentration effects on the recorded tTDR signal, based on a germanium sample measured with a modulation frequency of 1 MHz. Both (a) the temperature and (b) the carrier concentration affect (c) the refractive index, and multiplying the refractive index deviation by (d) the sensitivity and integrating gives (e) the measured signal. The real part of the signal is influenced by both the single-pulse response and the modulation-frequency response, and the imaginary part is primarily by the modulation-frequency response.

below. Literature values are used for heat capacities[27] with an assumed 10% uncertainty, and spot sizes are measured by analysis of photos of the laser spot. For the germanium sample, a lower magnification objective was used than for silicon, leading to a larger spot size, and the spot size was determined from a photo of the reflected laser, leading to uncertainty from setting the camera focus; for the silicon, the camera was placed in the sample location, minimizing this uncertainty. Multiple images were taken of each laser spot and the range of spot sizes found was used in calculating error bars on thermal conductivity.

TABLE I. Parameters affecting $\Delta V(t_{delay})$ after normalization.

Symbol	Property	Function of
Λ_z, Λ_r	Thermal conductivities	Sample
c_p	Heat capacity	Sample
D_z, D_r	Electrical diffusivities	Sample
s	Surface recombination velocity	Sample
E_g	Bandgap	Sample
τ	Carrier lifetime	Sample and measurement
α	Pump absorption rate	Sample and measurement wavelength
δ_1	Probe absorption depth	Sample and measurement wavelength
n	Index of refraction at the probe wavelength	Sample and measurement wavelength
$\frac{\partial n}{\partial N}/\frac{\partial n}{\partial T}$	Ratio of the carrier signal to the temperature signal	Sample and measurement wavelength
w_0, w_1	Pump and probe spot radii	Measurement
ω_0	Modulation frequency	Measurement
$h\nu$	Pump photon energy	Measurement
λ	Probe wavelength	Measurement

Assessment of these parameters leaves the carrier recombination time, the surface recombination velocity, the ratio $\frac{\partial n}{\partial N}/\frac{\partial n}{\partial T}$, and the thermal conductivity to be determined. Though we are unable to fit to all of these parameters simultaneously, only a narrow range of values was found that gave consistent results at all modulation frequencies, and these were used in the final fitting to thermal conductivity. We analyze the total magnitude of our tTDR signal, normalized to that just before the pump arrival.

Germanium

Best-fit values for germanium properties were found through an iterative fitting procedure, starting with expected literature values. The carrier recombination time and surface recombination velocity were perturbed, in turn, until high quality fits with consistent values across modulation frequency were found. The signal at small delay time is more sensitive to the ratio $\frac{\partial n}{\partial N}/\frac{\partial n}{\partial T}$ than that at longer delay time, so fits to the first nanosecond of data were used to determine $\frac{\partial n}{\partial N}/\frac{\partial n}{\partial T}$, and fits to the full dataset were used to determine the thermal conductivity.

The significantly larger best-fit surface recombination velocity compared to the literature value for germanium is not surprising,

Published under an exclusive license by AIP Publishing

TABLE II. Values of parameters used for fits. Ranges listed were used in the calculation of error bars and are the smaller of the assumed uncertainty of the measurement in which the value was found or the maximum range in which it was possible to find a good fit to the experimental data. See text for further description of ranges used and commentary on comparison to literature values.

Parameter	Value for Ge	Range for Ge	Literature values for Ge	Value for Si	Range for Si	Literature values for Si
c_p (J/m^3 K)[27]	1.70×10^6	1.53×10^6 to 1.87×10^6	1.70×10^6	1.66×10^6	1.49×10^6 to 1.83×10^6	1.66×10^6
D (m^2/s)	5.3×10^{-6}	5.25×10^{-6} to 5.35×10^{-6}	7.7×10^{-3} [28]	7.3×10^{-4}	6.6×10^{-4} to 7.9×10^{-4}	3.5×10^{-3} [29]
s (m/s)	80	72–104	0.8[30]	125	124–133	87–500[31]
τ (s)	1×10^{-5}	5×10^{-7} to 1×10^{-2}	7×10^{-7} [32]	9×10^{-8}	8.6×10^{-8} to 9.6×10^{-8}	3×10^{-9} [33]
α (1/m)	4.4×10^7	…	4.5×10^7 [34]	7.1×10^5	…	7.1×10^5 [34]
δ_1 (m)	2.3×10^{-7}	…	2.0×10^{-7} [34]	9.7×10^{-6}	…	9.7×10^{-6} [34]
n	4.72	…	4.71[34]	3.69	…	3.69[34]
$\frac{\partial n}{\partial N} / \frac{\partial n}{\partial T}$ (m^3 K)	-5.72×10^{-26}	-6.18×10^{-26} to -5.26×10^{-26}	-6×10^{-25} [35,36]	-7.54×10^{-24}	-12.3×10^{-24} to -8.69×10^{-24}	-9×10^{-25} [36,37]
Effective spot size (m)	2.1×10^{-5}	1.68×10^{-5} to 2.52×10^{-5}	…	7.6×10^{-6}	7.37×10^{-6} to 7.83×10^{-6}	…

as surface recombination is very sensitive to surface quality and our sample received no special surface treatment. The carrier recombination time estimated from the literature assumes a carrier concentration equal to that immediately following the pump incidence; the lower carrier concentration at longer delay times would lead to a longer recombination time, explaining the difference to our measured value. We repeated our measurements at laser powers lower than those reported here and did not see a significant difference in

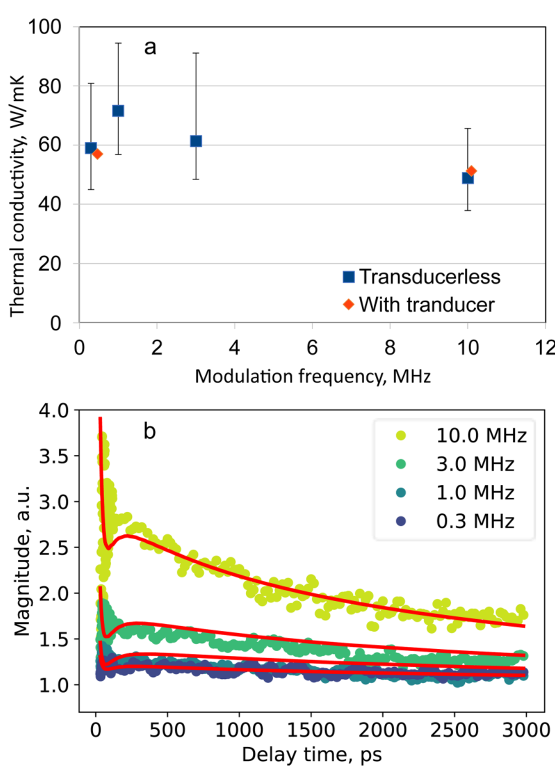

FIG. 7. Fitting results for germanium. (a) Fitted values of thermal conductivity. Error bars are found by perturbing input parameters within their uncertainties. (b) The overall fit of the model to the total magnitude of recorded tTDR data for each modulation frequency. The large signal at small delay times is caused by the dominance of the carrier response at those times.

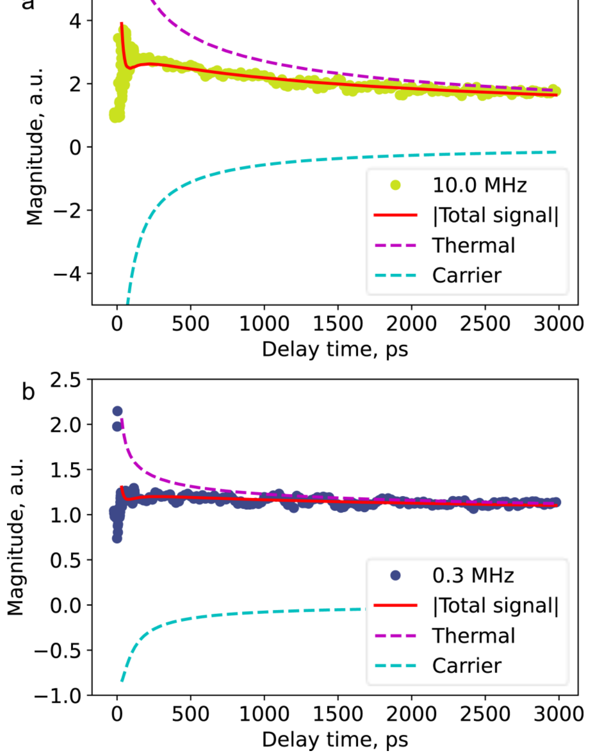

FIG. 8. Calculated thermal and carrier contributions to the magnitude of the total tTDR signal recorded for the Ge sample at (a) 10 and (b) 0.3 MHz. The total signal is the absolute value of the sum of the (positive) thermal contribution and the (negative) carrier contribution. The carrier effect is more significant at the higher modulation frequency, but the thermal signal is larger except at very small delay times.

Published under an exclusive license by AIP Publishing

normalized signal, despite the expected dependence of carrier recombination time on pulse energy due to the weak dependence of the final signal on the recombination time. The calculated literature value of $\frac{\partial n}{\partial N}/\frac{\partial n}{\partial T}$ relies on both estimation of $\frac{\partial n}{\partial T}$ based on data measured at longer wavelengths and on the validity of the Drude model for $\frac{\partial n}{\partial N}$, meaning that the difference from it to the best-fit value is not significant.

Once best-fit values for all parameters (as listed in Table II) were determined, uncertainties were assessed. Because of the numerical complexity of the model, our ability to consider the simultaneous effects of multiple parameters, for example, through the Monte Carlo method, was limited, and error bars were estimated based on the effects of each parameter individually. The uncertainties for the carrier recombination time and the surface recombination velocity were found by changing the value of each parameter individually until the model failed to find a good fit to the data, defined as a doubling of the residuals of the fit or a difference of more than 40% in values found for different modulation frequencies. The range of $\frac{\partial n}{\partial N}/\frac{\partial n}{\partial T}$ considered was that given by the fits for different modulation frequencies. The effect of the uncertainty in each input parameter was determined by repeating the fitting to thermal conductivity with that parameter modified to the limits of its uncertainty and recording the resultant change in fitted value, $\Delta\Lambda_i$ for parameter i. The

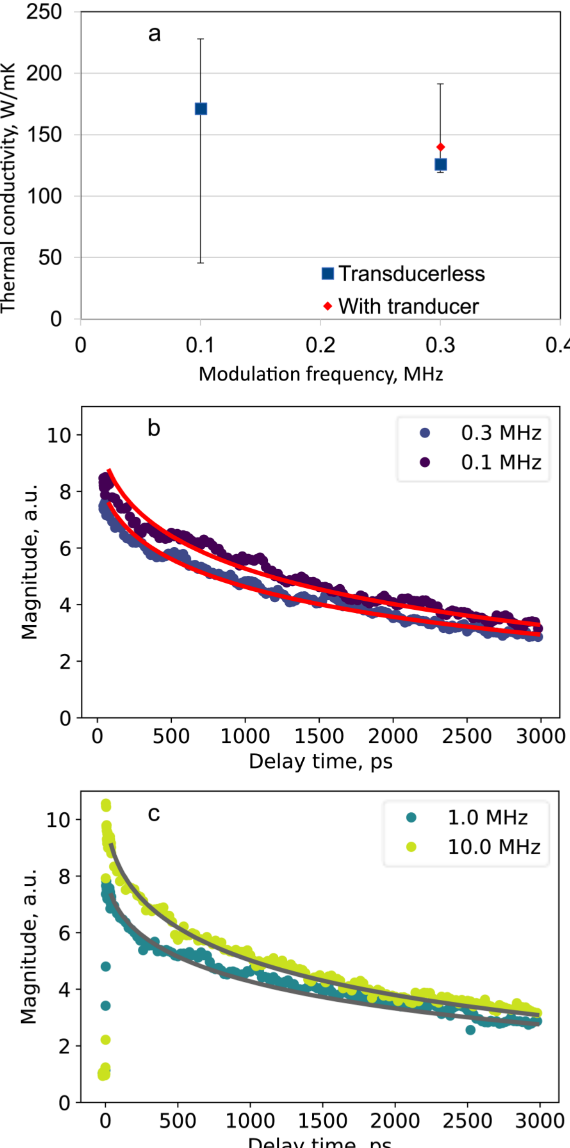

FIG. 9. Fitting results for silicon. (a) Fitted values of thermal conductivity. Error bars are found by perturbing input parameters within their uncertainties. We attribute the larger error bars at 0.1 MHz to the larger instrument noise at low frequency. (b) The overall fit of the model to the total magnitude of tTDR data for low modulation frequencies, where thermal conductivity was the fitting parameter. (c) The overall fit of the model to the total magnitude of tTDR data for higher modulation frequencies, where carrier properties were fit.

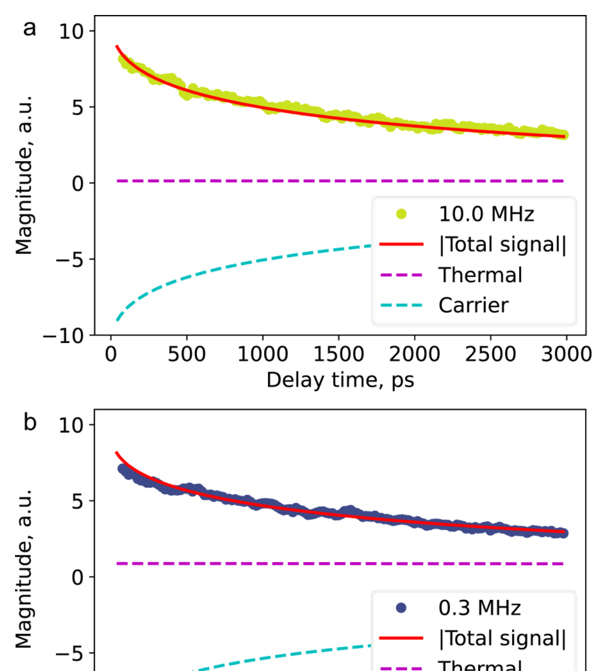

FIG. 10. Calculated thermal and carrier contributions to the total tTDR signal recorded for the Ge sample at (a) 10 and (b) 0.3 MHz. The total signal is the absolute value of the sum of the (positive) thermal contribution and the (negative) carrier contribution. The carrier effect dominates in both cases, but the thermal effect is non-negligible at low modulation frequency.

Published under an exclusive license by AIP Publishing

magnitudes of the error bars are found as

$$\Delta\Lambda_{tot} = \sqrt{\sum_i (\Delta\Lambda_i)^2}. \quad (32)$$

Fitting results for the germanium sample are shown in Fig. 7. Our average fitted thermal conductivity of 60 W/mK matches the value found by Maycock[38] and aligns well with the result we measured by standard TDTR of 51–57 W/mK. Over the tens of picoseconds to nanoseconds of delay time typical of a TDTR measurement, the model is a good fit.

As discussed above, the measured tTDR signal is a combination of thermal and carrier effects. In Fig. 8, we examine the relative components of the thermal and electrical signals for germanium. The measured signal is explained primarily by the thermal behavior at long delay times, but at short delay times, the carrier behavior is also relevant.

Silicon

Fits for the silicon sample, shown in in Fig. 9, were found through a similar procedure to those for the germanium sample. However, in contrast to the case of germanium, for silicon, the signal is dominated by the carrier response (Fig. 10) due to the much higher value of $\frac{\partial n}{\partial N}/\frac{\partial n}{\partial T}$ for the silicon sample. We attribute this to silicon having a weaker dependence of refractive index on temperature than germanium for measurements at 800 nm. Because of the dominance of the carrier response, we were only able to find fitting values for the thermal conductivity for the

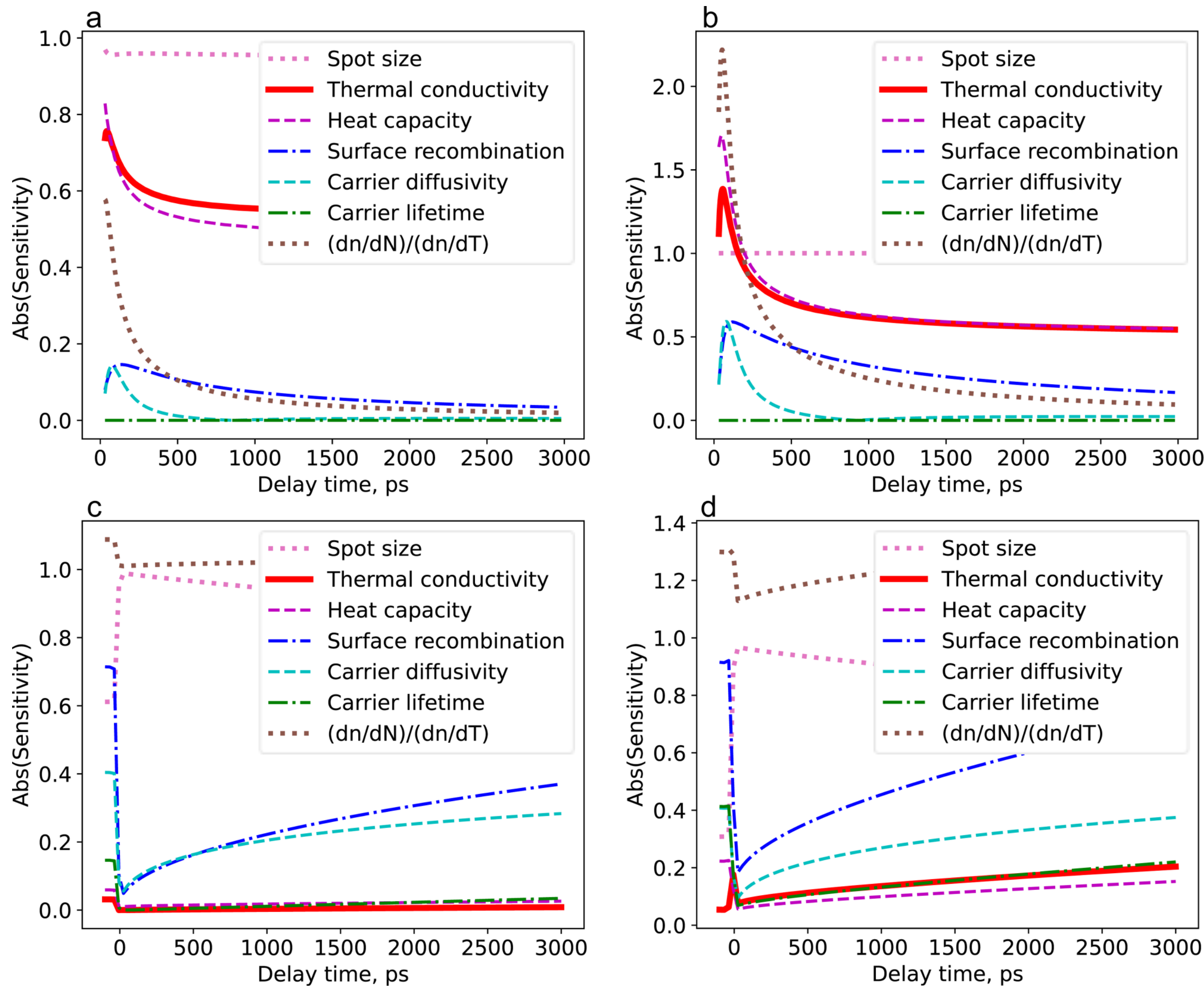

FIG. 11. Sensitivity plots for (a) Ge at 10 MHz modulation frequency, (b) Ge at 0.3 MHz, (c) Si at 10 MHz, and (d) Si at 0.1 MHz.

Published under an exclusive license by AIP Publishing

measurements at the lowest modulation frequencies, where the sensitivity to the thermal properties is strongest. We used the data collected at higher modulation frequency to determine the electrical diffusivity, carrier recombination rate, and surface recombination velocity by a similar iterative procedure to that used for the germanium fitting, and then fit $\frac{\partial n}{\partial N}/\frac{\partial n}{\partial T}$ and the thermal conductivity based on the low frequency data. Error bar calculations for the silicon sample were performed as for the germanium sample.

The best-fit value of the surface recombination velocity was within the range expected from the literature. As in germanium, the fitted carrier recombination rate was lower than expected from Auger recombination based on the initial carrier concentration, which we attribute to the lower carrier concentration at longer delay times. We did not observe a significant dependence of our signal on laser pulse energy, but this does not rule out a dependence of carrier recombination time on pulse energy as the final signal is not very sensitive to recombination time, especially, when that time is larger, as occurs at lower pulse energies. Our estimate of $\frac{\partial n}{\partial N}/\frac{\partial n}{\partial T}$ for silicon is similar to that of germanium, whereas our observed values are quite different, which highlights the limitations of our method for estimating $\frac{\partial n}{\partial N}/\frac{\partial n}{\partial T}$.

Despite the larger uncertainty caused by the lower sensitivity to thermal conductivity and higher noise in our system at low frequency, our average fitted result for the thermal conductivity of silicon of 148 W/mK compares well to the literature value of 149 W/mK[12] and to our result from standard TDTR of 140 W/mK. We highlight that our consideration of photoexcited carriers allows our model to describe the behavior of this sample, unlike the model presented by Qian *et al.*, which fails to fit their experimental data for silicon.[16] We anticipate that laser wavelengths other than those used here may allow measurement with lower uncertainty: a shorter pump wavelength would provide more thermal energy per incident photon, without increasing the initial carrier density, and a different probe wavelength might provide a higher $\frac{\partial n}{\partial T}$ and so more sensitivity to thermal changes.

Sensitivity analysis

To better understand the properties of our model, we perform a quantitative sensitivity analysis. Defining the sensitivity to a parameter x as $S_x = \frac{\partial \ln R}{\partial \ln x}$ and comparing the relative sensitivities of various parameters, we can establish how strongly each parameter influences our result. Results for Ge and Si at high and low modulation frequency are shown in Fig. 11.

For the germanium sample, the sensitivity to thermal conductivity is higher than that to other parameters except for the spot size and heat capacity. At low delay times and high frequencies, $\frac{\partial n}{\partial N}/\frac{\partial n}{\partial T}$ has a significant impact on the signal, but this sensitivity is decreased at larger delay times. Sensitivity to carrier lifetime is negligible, implying that surface recombination occurs significantly faster than bulk recombination in this sample. Though the sensitivity to spot size is larger than that to thermal conductivity, the fact that it is nearly constant with delay time, and we fit to normalized data means that uncertainty in spot size has minimal effect on the fitting result. As long as the heat capacity of the sample is well known, fitting to the thermal conductivity will be reliable.

By contrast, the sensitivity to thermal conductivity in the silicon sample is very small—indeed, negligible at high frequency. As shown in Fig. 10 and indicated by the high sensitivity to $\frac{\partial n}{\partial N}/\frac{\partial n}{\partial T}$, the sample response is determined primarily by the carrier response, not the thermal one. To have any confidence in a value measured for the thermal conductivity, we took advantage of the minimal sensitivity to thermal properties at high frequency and fit to the carrier diffusivity, carrier recombination rate, and surface recombination velocity, increasing our confidence in our input for fits at low frequencies. Thus, even though the fits at 0.1 and 0.3 MHz are still dominated by the carrier properties, we have sufficient confidence in the values of those properties to determine a thermal conductivity.

CONCLUSIONS

The dominant noncontact methods of measuring thermal conductivity, TDTR and FDTR, generally require the use of a metal film transducer. However, the use of a transducer complicates the measurement and can restrict access to or reduce sensitivity to certain material properties of interest. In this paper, we demonstrate that time-domain transient reflectivity measurements of the thermal properties of semiconductors can be made without the use of a transducer. We present a model for both carrier and thermal responses to heating with, and measurement by, laser spots of finite dimension and non-zero penetration depth. We show that the model accurately describes the signal from direct measurements of germanium and silicon samples. Though we do not explore fully the possibility in this work, we anticipate that this result will be easily extended to the measurement of samples, which cannot be easily measured with a transducer, for example, ultra-thin films or suspended membranes.

ACKNOWLEDGMENTS

Qinshu Li and Professor Bo Sun provided the standard TDTR measurements of germanium, Dr. Danqing Wang performed Hall effect measurements, and Professor Joel Ager III provided the germanium sample. This work was supported by the Electronic Materials Program and made use of the Molecular Foundry, both in the Lawrence Berkeley National Laboratory, and was supported by the Director, Office of Science, Office of Basic Energy Sciences, Materials Sciences, and Engineering Division of the U.S. Department of Energy under Contract No. DE-AC02-05CH11231. S.W. was supported by the Department of Defense (DoD) through the National Defense Science & Engineering Graduate (NDSEG) Fellowship Program.

AUTHOR DECLARATIONS

Conflict of Interest

The authors have no conflicts of interest to declare.

DATA AVAILABILITY

The data that support the findings of this study are available from the corresponding author upon reasonable request.

Published under an exclusive license by AIP Publishing

REFERENCES

[1]D. Fournier, M. Marangolo, and C. Fretigny, J. Appl. Phys. **128**, 241101 (2020).
[2]M. D. Dramicanain, Z. D. Ristovski, P. M. Nikolic, D. G. Vasiljevic, and M. Todorovic, Phys. Rev. B **51**, 226 (1995).
[3]V. A. Sablikov and V. B. Sandomirskii, Phys. Status Solidi B **120**, 471 (1983).
[4]D. Fournier, C. Boccara, A. Skumanich, and N. M. Amer, J. Appl. Phys. **59**, 787 (1986).
[5]D. Fournier and A. C. Boccara, Mater. Sci. Eng. B **5**, 83 (1990).
[6]R. G. Stearns and G. S. Kino, in *Thermal Wave Phenomena in Semiconductors*, edited by A. Mandelis (North Holland Publishing Company, New York, 1987).
[7]R. E. Wagner and A. Mandelis, in *Photoacoustic and Photothermal Phenomena III: Proceedings of the 7th International Topical Meeting*, edited by D. Bicanic (Springer-Verlag, Berlin, 1992), pp. 372–374.
[8]D. H. Hurley, O. B. Wright, O. Matsuda, and S. L. Shinde, J. Appl. Phys. **107**, 023521 (2010).
[9]I. A. Vitkin, C. Christofides, and A. Mandelis, J. Appl. Phys. **67**, 2822 (1990).
[10]A. Salnick and J. Opsal, Rev. Sci. Instrum. **74**, 545 (2003).
[11]D. G. Cahill, Rev. Sci. Instrum. **75**, 5119 (2004).
[12]A. J. Schmidt, R. Cheaito, and M. Chiesa, Rev. Sci. Instrum. **80**, 094901, (2009).
[13]C. A. Paddock and G. L. Eesley, J. Appl. Phys. **60**, 285 (1986).
[14]L. Wang, R. Cheaito, J. L. Braun, A. Giri, and P. E. Hopkins, Rev. Sci. Instrum. **87**, 094902 (2016).
[15]R. Rosei and D. W. Lynch, Phys. Rev. B **5**, 3883 (1972).
[16]X. Qian, Z. Ding, J. Shin, A. J. Schmidt, and G. Chen, Rev. Sci. Instrum. **91**, 064903 (2020).
[17]T. Tanaka, A. Harata, and T. Sawada, J. Appl. Phys. **82**, 4033 (1997).
[18]D. Guidotti and H. M. Van Driel, Appl. Phys. Lett. **47**, 1336 (1985).
[19]G. Mak and W. W. Rühle, Phys. Rev. B **52**, 584 (1995).
[20]J. Yang, E. Ziade, and A. J. Schmidt, J. Appl. Phys. **119**, 095107 (2016)
[21]K. Misiakos and D. Tsamakis, J. Appl. Phys. **74**, 3293 (1993).
[22]F. J. Morin and J. P. Maita, Phys. Rev. **94**, 1525 (1954).
[23]T. H. Geballe and G. W. Hull, Phys. Rev. **94**, 1134 (1954).
[24]T. H. Geballe and G. W. Hull, Phys. Rev. **98**, 940 (1955).
[25]C. Thomsen, H. T. Grahn, H. J. Maris, and J. Tauc, Phys. Rev. B **34**, 4129 (1986).
[26]A. Rosencwaig, in *Photoacoustic and Thermal Wave Phenomena in Semiconductors*, edited by A. Mandelis (North Holland Publishing Company, New York, 1987).
[27]*CRC Handbook of Chemistry and Physics*, 102nd ed., edited by J. R. Rumble (CRC Press, Boca Raton, 2021).
[28]P. P. Debye and E. M. Conwell, Phys. Rev. **93**, 693 (1954).
[29]C. Canali, F. Nava, and L. Reggiani, *Hot-Electron Transport in Semiconductors* (Springer, Berlin, 1985), pp. 87–111.
[30]D. T. Stevenson and R. J. Keyes, Physica **20**, 1041 (1954).
[31]D. Baek, S. Rouvimov, B. Kim, T. C. Jo, and D. K. Schroder, Appl. Phys. Lett. **86**, 112110 (2005).
[32]S. Dominici, H. Wen, F. Bertazzi, M. Goano, and E. Bellotti, Appl. Phys. Lett. **108**, 211103 (2016).
[33]R. A. Sinton and R. M. Swanson, IEEE Trans. Electron Devices **34**, 1380 (1987).
[34]D. E. Aspnes and A. A. Studna, Phys. Rev. B **27**, 985 (1983).
[35]B. J. Frey, D. B. Leviton, and T. J. Madison, Proc. SPIE **6273**, 62732J (2006).
[36]W. G. Spitzer and H. Y. Fan, Phys. Rev. **106**, 882 (1957).
[37]G. E. Jellison and H. H. Burke, J. Appl. Phys. **60**, 841 (1986).
[38]P. D. Maycock, Solid State Electron. **10**, 161 (1967).

Published under an exclusive license by AIP Publishing